Regime Transitions in Fractions of Isotactic Polypropylene†

Stephen Z. D. Cheng,* James J. Janimak, and Anqiu Zhang‡

Institute and Department of Polymer Science, College of Polymer Science and Polymer Engineering, The University of Akron, Akron, Ohio 44325-3909

H. N. Cheng

Research Center, Hercules Inc., Wilmington, Delaware 19894. *Received March 31, 1989; Revised Manuscript Received May 23, 1989*

ABSTRACT: Crystal growth rates of spherulites or axialites of low molecular mass (MW = 15 000) and high molecular mass (MW = 300 000) isotactic polypropylene (i-PP) fractions crystallized from the melt have been investigated in an extensive supercooling range (20–70 K). On the basis of the regime theory, a transition between regimes I and II is found at $\Delta T \cong 37$ K for the low molecular mass fraction and a transition between regimes II and III is at $\Delta T \cong 48$ K for both low and high molecular mass fractions of i-PP. Accordingly, the morphological changes observed by a polarized optical microscope at the supercooling range in the vicinity of regime transitions have been examined. The morphological change in this supercooling range does not correlate to the regime transitions.

Introduction

In 1975, Hoffman and his co-workers[1] found a regime behavior (regimes I and II) for the case of melt crystallization in polyethylene (PE) fractions. The occurrences were interpreted by two different nucleation mechanisms.[2-7] A new crystallization regime (regime III) develops at high supercooling when the niche distance is reduced to approximately several times the width of a polymer chain stem. This regime was expected by Hoffman[5] and Phillips[8] in 1979 and suggested and formulated by Hoffman in 1983.[7]

Further studies have indicated that the development of such regime transitions can be anticipated as a function of molecular mass,[9] polydispersity,[10] chemical structure and therefore flexibility of the chain,[11] etc. Until now, four polymers have been sufficiently studied over an extensive molecular mass composition, namely, PE,[1,5-7] *cis*-polyisoprene (*cis*-PI),[10] poly(ethylene oxide) (PEO),[12] and poly(3,3-dimethylthietane) (PDMT),[13] to exhibit all those crystallization regimes. The lineal growth rates of polymeric spherulites or axialites can be treated in much the same way as their constituent lamellae and hence be defined in terms of a well-known conventional equation:[14]

$$v_c = v_0(\Delta T) \exp[-U^*/R(T_c - T_\infty)] \exp[-K_g/T_c(\Delta T)f] \quad (1)$$

The term v_0 involves all the terms that are temperature-insensitive. U^* in the first exponential in eq 1 represents the activation energy that governs the short distance diffusion of the crystalline element across the phase boundary. T_∞ is the temperature below which such motion ceases, namely, $T_\infty = T_g - 30$ K. These quantities are derivable from the WLF equation analyses. It was also reported that the universal value for U^* is 6.28 kJ/mol.[14] The second exponential term in eq 1 represents the Gibbs free energy contribution for growth of a critical size surface nucleus. It is dependent upon the degree of supercooling, ΔT. The factor f is termed the correcting factor for variations in the heat of fusion, Δh_f, with temperature and is usually prescribed to equal to $2T_c/(T_c + T_m^0)$. Finally, in this term, the parameter K_g can be expressed by

$$K_g(\mathrm{I}) = 4b_0\sigma\sigma_e T_m^0/k(\Delta h_f) \quad (2)$$

in regime I, where σ and σ_e are the lateral and fold surface free energies, respectively, k is the Boltzmann constant, and b_0 the layer thickness.

In regime II, the parameter K_g is

$$K_g(\mathrm{II}) = 2b_0\sigma\sigma_e T_m^0/k(\Delta h_f) \quad (3)$$

and in regime III, one has

$$K_g(\mathrm{III}) = 4b_0\sigma\sigma_e T_m^0/k(\Delta h_f) \quad (4)$$

under the assumption of surface nucleation model.

Taking the logarithm of eq 1, one obtains

$$\log v_c = \log v_0 + \log(\Delta T) - U^*/[2.303R(T_c - T_\infty)] - K_g/[2.303T(\Delta T)f] \quad (5)$$

The overall picture of regime transitions can be shown by a plot of $\log v_c + U^*/[2.303R(T_c - T_\infty)] - \log(\Delta T)$ vs $1/[T(\Delta T)f]$, which exhibits two intersecting straight lines with two slope differences close to two as required by eq 2–5. On the basis of this treatment, one can see that the major hindering effect or conversely driving force for polymer crystal growth is the surface free energy.

Regime behavior has also been realized in some polymer systems besides PE, *cis*-PI, PEO, and PDMT. The regime I/II transition is known in the melt-crystallized poly(L-lactic acid)[15] and poly(1,3-dioxolane)[16] as well as in PE single crystals formed from dilute solution.[17] The regime II/III transition has been observed in poly(oxymethylene),[7,18] poly(pivalolactone),[19] poly(3-hydroxybutyrate),[20] isotactic polypropylene (i-PP),[21] and poly(*p*-phenylene sulfide).[11]

In the early 1980s, the now late Dr. Sadler developed an alternate explanation for polymer crystal growth based on a continuous growth model on a rough surface.[22] He proposed that there should be an entropy barrier in front of a growth surface instead of a nucleation barrier. In one of his last papers, an attempt was made to interpret the regime transitions.[22,23]

For i-PP, Allen and Mandelkern reported recently a regime I/II transition at $\Delta T \simeq 56$ K (the equilibrium melting temperature of i-PP crystals of 481.2 K was used).

† Part of a dissertation to be submitted to the Graduate School, The University of Akron, by J. J. Janimak in partial fulfillment of the requirements for the Ph.D. degree in Polymer Science.

‡ On leave from China Textile University, Shanghai, China.

0024-9297/90/2223-0298$02.50/0

Table I
Characteristic Analysis of i-PP Fractions

sample designatn	isotacticity	$\bar{M}_n$	$\bar{M}_w/\bar{M}_n$	mol length,[a] nm
i-PP15k	>0.99	15 000	1.7	77.17
i-PP300k	>0.99	300 000	2.0	1543.5

[a] The molecular length was calculated by $\bar{M}_n/[3 \times 42.08/0.6495]$, where 3 represents the number of repeating units per turn in chain conformation in the crystalline state, 42.08 is molecular mass per mole, and 0.6495 nm is the c^* axis of the *i*-PP α-crystal unit cell.

They also found that the regimes do not serve as boundaries between distinct morphological forms.[24]

Our recent experimental results of crystal growth rates in two well-characterized fractions of i-PP (α-form) have exhibited such regime behavior. After the measurements of growth rates of spherulites or axialites in i-PP fractions crystallized from the melt over a wide supercooling range (20–70 K), a regime I/II transition has been observed at $\Delta T \cong 37$ K for the low molecular mass (MW = 15 000) fraction. In both the cases of low molecular mass (MW = 15 000) and high molecular mass (MW = 300 000) fractions, a regime II/III transition is barely apparent at $\Delta T \cong 48$ K. For all cases, regimes II/III and regimes I/II produce slope ratios of approximately two, with a margin of error in the vicinity of ±0.15. The morphological change in this supercooling range does not correlate to the regime transitions.

Experimental Section

Materials and Samples. The i-PP samples used in this investigation were kindly supplied by Hercules Inc. Their tacticities, molecular mass, and polydispersities are summarized in Table I. Their molecular lengths are also listed in this table. Both the low and high molecular mass i-PP fractions are designated to be i-PP15k and i-PP300k, respectively.

It is generally known that in i-PP polymorphism leads to three major different crystal forms: α-, β-, and γ-forms with monoclinic, hexagonal, and triclinic crystal lattices, respectively. The lowest energy chain conformation of i-PP in the crystalline state is the 2*3/1 helix. On the basis of the classification of spherulitic morphology observed by Padden and Keith,[25] four types of spherulites can be distinguished in which types I and II belong to the α-form. Distinction between types I and II was defined by the difference in their respective birefringence values: positive for the former and negative for the latter. Recently, Norton and Keller[26] related these corresponding changes in birefringence to ascribed morphological modifications from predominant branching lamellae to radiating lamellae. Types III and IV spherulites are inherent in the much rarer β-form. They appear sporadically and only under certain constraints of isothermal crystallization and nonisothermal crystallization and are noticeable by their high negative birefringence and from their intense optical luminescence. In this paper, we will focus only on the crystal growth rates of i-PP in its α-form.

Instrumentation. Differential Scanning Calorimeter (DSC). All the samples were measured with an updated computer interfaced Perkin-Elmer DSC2. The DSC was calibrated following the standard procedures. Both temperature and heat-flow levels were corrected by using standard materials. Measurements of the phase transitions were performed at a heating rate of 10 K/min. Typical sample weights were 3–6 mg. All experiments were carried out under dry nitrogen.

Polarized Optical Microscope (POM). Polarized optical microscopy observations of isotactic polypropylene were carried out by using a Leitz-Wetzlar POM with 800× magnification and a Mettler FP52 hot stage under an atmosphere of dry nitrogen at atmospheric pressure. The hot stage was calibrated with standard, sharp melting substances around the temperature range of interest. The sample films were pressed between a coverslip and a microscope slide to about 15 μm thickness as controlled by an aluminum film wedge. The linear crystal growth rates were measured during the spherulitic or axialitic growth. The linearity was assured by successive measurements of the growth rate at various time intervals prior to impingement effects. Five measurements at each temperature were carried out, and the standard deviation was ±2%. Photographs were taken with a 35-mm Nikon camera. The crystallization time, t_c, was recorded by a chronograph timer. The observed scales in the POM were calibrated by using a graduated grid standard of 0.1-mm intervals into 1-μm divisions.

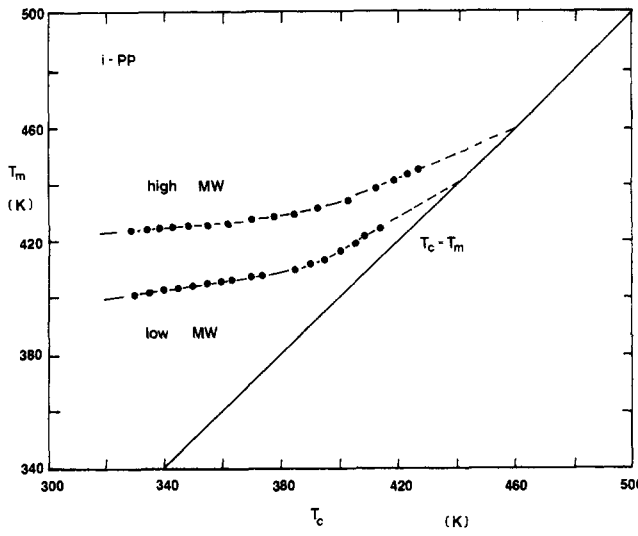

Figure 1. Relationship between the melting temperature and isothermal crystallization temperature of i-PP15k. The extrapolation based on Hoffman and Weeks indicates an equilibrium melting temperature of 443.2 K.

Small Angle X-ray Scattering (SAXS). Small angle X-ray scattering investigations were carried out with a Rigaku Denki rotaflex RU-200 D/max rB generator with a 12-kW rotating anode as a source of the incident X-ray beam. The point-focused beam is monochromatized with a graphite crystal, and a Ni filter was adapted to a pulse height analyzer to produce Cu Kα radiation. The SAXS goniometer was modified with a 505-mm vacuum chamber. A Braun OED 50-mm positional sensitive detector was attached with 4096 channels. Lorentz correction of SAXS results was done by multiplying the intensity (counts per second) by s^2 ($s = 2 \sin \theta/\lambda$, where λ is wavelength of X-ray, 1.541 78 Å). A temperature controller was added on to the SAXS apparatus for thermal measurements. The precision of the controller was ±0.5 K in the temperature range studied here. Programmed heating and cooling can be performed under control. The i-PP samples were measured on the SAXS apparatus at their isothermal crystallization temperatures. To calculate the lamellar thickness, a correlation-function method reported by Tanabe et al. was applied.[27]

Results and Discussion

Equilibrium Melting Temperatures of i-PP Fractions. Two different methods were applied to evaluate the equilibrium melting temperatures of the i-PP fractions, which are molecular mass dependent. The first approach is the extrapolation of the onset melting temperature, T_m, with respect to the isothermal crystallization temperature, T_c, based on the description of Hoffman and Weeks.[28] Figure 1 shows such extrapolations for both the i-PP15k and i-PP300k. This leads to a temperature of 443.2 K for i-PP15k as its equilibrium melting temperature, T_m^0. For i-PP300k, an equilibrium melting temperature of 458.2 K can be found.

Figure 2 represents the relationship between the reciprocal of i-PP lamellar thickness crystallized at different isothermal temperatures and their melting temperatures. It is a combination of both SAXS and DSC meth-

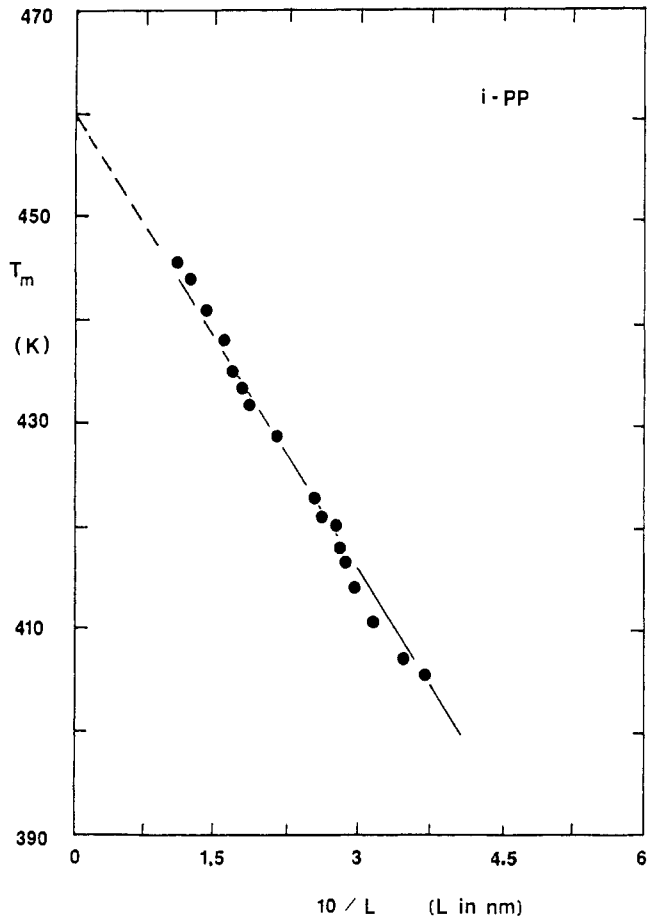

Figure 2. Relationship between the recriprocal lamellar thickness ($1/l$) and their corresponding melting temperature of i-PP fractions. The extrapolation indicates an equilibrium melting temperature at infinitely large crystals at 458.2 K.

ods. One can find that the extrapolation of this relationship leads to an equilibrium melting temperature of 458.2 K at $1/l = 0$.[29] When one considers the finite length of the molecules for i-PP15k, it is 453.9 K on the basis of the extrapolation. We know that such extrapolation assumes that in the case of laterally large lamellae, the only surfaces contributing significantly to the free enthalpy of the crystal are the top and bottom surfaces, so that the Thomson–Gibbs equation can be simplified to[29]

$$T_m = T_m^0(1 - 2\sigma_e/l\Delta h_f) \quad (6)$$

where T_m^0 is the melting temperature of the infinitely large crystal (the equilibrium melting temperature), σ_e the top and bottom specific surface free energy, l the lamellar thickness, and Δh_f, as before, the bulk heat of fusion per cubic centimeter. When one applies this equation, it has to be noticed that the fold surface free energy, σ_e, is generally different from the surface free energy that is contributed by chain ends. The difference between these two surface free energies may lead to a deviation of the equilibrium melting temperatures for both crystals with different types of top and bottom surfaces. Comparing Figure 2 with Figure 1, the two extrapolations are about 10.7 K apart. In order to eliminate the 10.7 K difference, one has to assume that the surface free energy that contains the most chain ends is about 247 erg/cm^2. This is about 3.5 times higher than the fold surface free energy ($\sigma_e \cong 70$ erg/cm^2 obtained from Figure 2 through eq 6).

Although our extrapolation data show the equilibrium melting temperature of i-PP is 458.2 K; other extrapolated melting temperatures from 456.2 K to 493.2 K have been reported. The data by Fatou,[30] for example, yield a value of 481.2 K as the best extrapolated melting temperature. At this moment, the equilibrium melting temperature of i-PP is still somewhat uncertain.

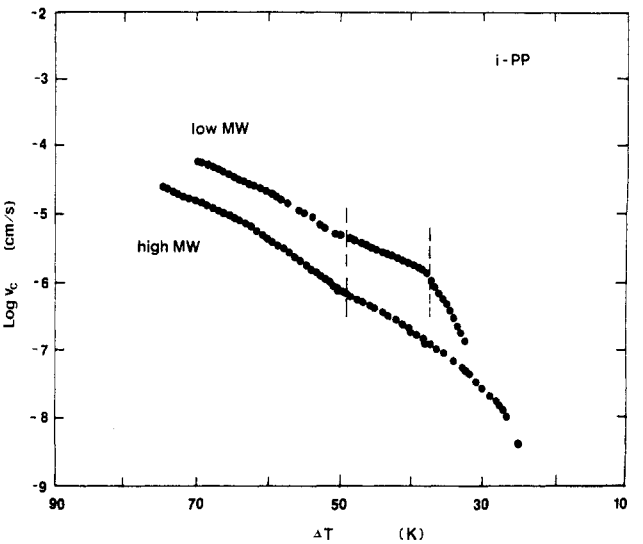

Figure 3. Relationship between the logarithmic crystal growth rate (log v_c) and supercooling for both low and high molecular mass i-PP fractions. The vertical dashed lines are those crossover points (see text). The equilibrium melting temperatures used here are 443.2 K for i-PP15k and 458.2 K for i-pp300k, respectively.

The regime III/II transition data we found ($\Delta T = 48$ K) is very close to the data reported by Clark and Hoffman[21] ($\Delta T = 49$ K). On the other hand, on the basis of Allen and Mandelkern's data, the regime II/I transition occurs at $\Delta T = 56$ K when $T_m^0 = 481.2$ K was used.[24] If one would apply $T_m^0 = 458.2$ K, that transition could be observed at $\Delta T = 37$ K, which is essentially the same as the data we found.

Crystal Growth Rates and Regime Analyses. Two sets of linear crystal growth rates are shown in Figure 3 as functions of their respective supercooling. For i-PP15k, one can find two crossover points. One is at $\Delta T = 48$ K, and the other $\Delta T = 37$ K. The second one is mainly recognized by the change of the slopes below and above $\Delta T = 37$ K. On the other hand, only one crossover point can be distinguished for i-PP300k, which is at $\Delta T = 48$ K. At low supercooling, no clear change of slope can be observed.

First of all, from the convex shapes of the curves shown in Figure 3 one can consider to apply the regime theory suggested by Hoffman, Lauritzen, and others[1-9,14] as shown in eq 1–5. Figure 4 represents the relationship betwen $\log v_c - \log \Delta T + U^*/[2.303R(T_c - T_\infty)]$ and $1/[T_c(\Delta T)f]$. For i-PP15k, three regimes are very clear: regime III at high supercooling, regime II at intermediate supercooling, and regime I at low supercooling. The supercoolings of regime transitions are at 48 and 37 K, respectively. Only one regime transition can be observed in i-PP300k at $\Delta T = 48$ K, indicating a regime III/II transition. In these regime analyses, we used $T_\infty = T_g - 30$ K, namely, 237.0 K for i-PP15k and 239.6 K for i-PP300k. $T_m^0 = 443.2$ K for i-PP15k, and 458.2 K for i-PP300K. The value of Δh_f is quoted to be 8.3 kJ/mol, and finally, the "universal" constant for U^* of 6.28 kJ/mol is applied.

Table II lists all the kinetic data of crystal growth for the two fractions. It is evident that all the ratios of the slopes between two neighboring regimes are in the vicin-

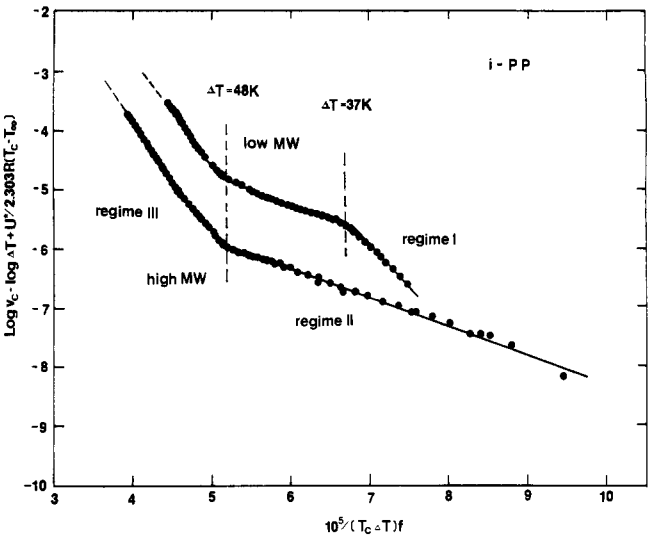

Figure 4. Plot of $\log v_c + V^*/[2.303R(T_c - T_\infty)] - \log(\Delta T)$ vs $1/[T(\Delta T)f]$ for both low and high molecular mass i-PP fractions. The low molecular mass fraction, i-PP15k, shows three regimes, and the high one, i-PP300K, two regimes.

ity of two (Table II), indicating the validity of present nucleation theory. From the slopes, one can calculate the products of lateral and fold surface free energies, $\sigma\sigma_e$, and they are in the range of 600~800 erg^2/cm^4 along (110) growth planes. Assuming the lateral surface free energy is 11.5 erg/cm^2, the fold surface free energies are thus between 52 and 70 erg/cm^2 on the basis of the derivation of the work of chain folding from the fold surface free energy by

$$q = 2\sigma_e a_0 b_0 \tag{7}$$

where $a_0 b_0$ represents the cross-sectional area of the polymer chain [0.344 nm^2 on (110) growth plane]. The values of q are also listed in Table II and are all in the vicinity of 25 kJ/mol, indicating a flexible chain nature of i-PP molecules. One can also find that the value of q for i-PP300k is about 30% lower than that of i-PP15k. Presumably this effect is caused by chain folding irregularities introduced by chain ends for the low molecular mass i-PP fraction, since for i-PP15k, the number of folds per molecule is rather small. For example, one molecule has about six to seven folds if one stem travels 10 nm.

According to the recent derivation of Hoffman and Miller,[31] the substrate length L can be estimated semiquanitatively by knowing the behavior of regime I and regime II crystal growth. It is thus possible for us to undergo this estimation for i-PP15k. Nevertheless, some changes must be made to eq 1 or 5, namely, the term of $-U^*/[2.303R(T_c - T_{inf})]$ should be rewritten by $Q_D^*/2.303RT_c$. Here Q_D^* is the enthalpy of reptation, which can be determined by the relationship between the self-diffusion coefficient and reciprocal temperature. At this moment, we cannot obtain a value for i-PP15k. Attempts to determine this value by our own measurement via pulse gradient spin echo (PGSE) NMR method are being currently undertaken. Therefore, the estimation of L will appear elsewhere.

Our data suggest that for i-PP a maximum molecular mass exists beyond which regime I growth will not be observed. A similar situation has been reported in the cases of PE[1] and *cis*-PI.[10] On the other hand, the regime II/I transition can also be smeared by broad molecular mass distribution, such as in PE case.[1] A further complication for i-PP is introduced by different degrees of tacticity. At this moment, a confident conclusion about the absence of regime I growth for i-PP300k is still awaited.

Table II
Kinetic Data of Crystal Growth of i-PP Fractions

sample designatn	regime	$10^{-5} K_g$, K^2	$\sigma\sigma_e$, erg^2/cm^4	q,[a] kJ/mol	ratio[b]
i-PP15k	I	2.996	731	26.3	1.86
	II	1.607	784	28.2	1.99
	III	3.196	779	28.0	
i-PP300k	II	1.250	590	21.2	2.04
	III	2.554	602	21.7	

[a] The calculation assumes σ = 11.5 erg/cm^2. [b] The values of ratio between two neighboring regimes are $K_g(I)/K_g(II)$ and $K_g(III)/K_g/(II)$.

Morphological Changes during Regime Transitions. During our measurements of the linear crystal growth rates of i-PP fractions via POM, we have observed gradual morphological changes which appear not to correlate with the regime transitions. Correspondingly the morphological differences were coupled with the measurement of birefringence for both i-PP15k and i-PP300k. Combining both textural observations as well as birefringence measurements, one can now differentiate the different spherulitic types according to the classification system of Padden and Keith.[25] Figure 5, parts a–e, indicates such changes at five distinct supercoolings for i-PP15k, as an example. Figure 5a represents a typical spherulite texture of the monoclinic α-crystal form of i-PP at ΔT = 59 K, which falls into the regime III category. Figure 5b represents a similar pattern to that of Figure 5a at ΔT = 51 K. The change in birefringence gradually diminishes from being wholly positive in Figure 5a to only slightly positive in Figure 5b. Figure 5c is at ΔT = 46 K, and population of spherulites grown at this supercooling exhibited a slightly negative birefringence and thence can be placed into Padden and Keith type II spherulite category.

Bassett and Olley have elucidated the origins for such birefringence and textural type patterns, as being responsible to complex cross-hatching mechanisms.[32] Further support of this phenomenon has been provided by Norton and Keller[26] and Lotz and Wittmann.[33] The behavior pattern of the cross-hatching arises from the dominant lamellae crisscross markings, at near orthogonal conditions (= 80.7° to their {001} crystal plane). The radial lamellae yield negative birefringence, and the tangential lamellae give rise to positive birefringence. With decreasing supercooling, the population of the tangential lamellae reduces.[26] One can thus observe the birefringence change with supercooling. In Figure 5d at ΔT = 39 K, the dominant morphology is still the spherulite with a more sheaflike texture. In Figure 5e at ΔT = 33 K, the morphology is extensively more open. One could classify the overall morphology with two-dimensional axialites. Bassett and Olley[32] have also found similar modifications as determined via transmission electron microscopy (TEM). They clearly identified that at the high crystallization temperatures of about 428.2 K the cross-hatching ceases to persist, such that simple sheaflike structures become the building blocks for the two-dimensional axialitic growth. The changes in birefringence at this supercooling intensifies from being slightly negative in nature to moderately negative in magnitude. Nevertheless, it must be pointed out that the appearance of such axialites does not necessarily relate to the regime II/I transition since similar texture can also be found in the case of i-PP300k crystallized at low supercooling, which does not exhibit the regime II/I transition.

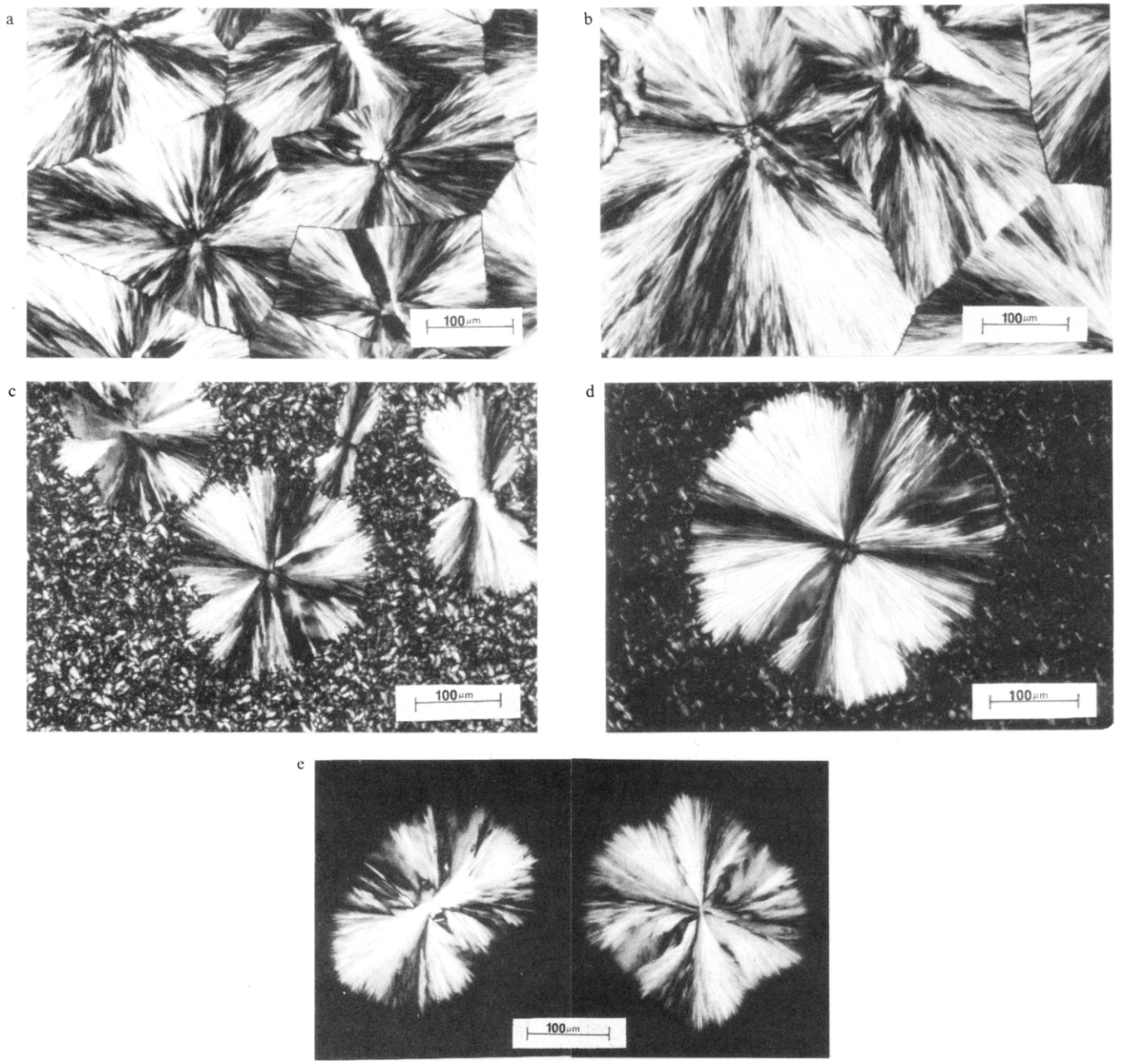

Figure 5. Crystalline morphology of i-PP15k at different supercoolings: (a) ΔT = 59 K; (b) ΔT = 51 K; (c) ΔT = 46 K; (d) ΔT = 39 K; (e) ΔT = 33 K. Note that between (b) and (c), transition between regimes II and III occurs, and between (d) and (e), transition between regimes II and I appears.

Conclusions

On the basis of our knowledge, this is the first time the observation of all three regimes in one i-PP fraction (i-PP15k) is reported. Detailed regime analyses indicate a regime III exists above ΔT = 48 K, a regime II exists in between ΔT = 48 K and 37 K, and below ΔT = 37 K, a regime I crystal growth appears. In the case of high molecular mass fractions, such as i-PP300k, only two regimes can be observed, namely, regimes III and II. The ratios between two neighboring regimes are close to two. Our morphological study for i-PP15k has shown that both texture and birefringence do not represent correlation with the regime change.

Acknowledgment. This research was partially supported by a Research Challenge Grant of Ohio Board Regents through the University of Akron. An extensive discussion of this topic with Dr. J. D. Hoffman is acknowledged. We also would like to thank P. A. Giusti for his continuous assistance in microscopy.

Registry No. i-PP, 25085-53-4.

References and Notes

(1) Hoffman, J. D.; Frolen, L. J.; Ross, G. S.; Lauritzen, J. I., Jr. *J. Res. Natl. Bur. Stand., Sect. A* **1975**, *79A*, 671.
(2) Lauritzen, J. I., Jr. *J. Appl. Phys.* **1973**, *44*, 4353.
(3) Lauritzen, J. I. Jr.; Hoffman, J. D. *J. Appl. Phys.* **1973**, *44*, 4340.
(4) Frank, F. C. *J. Cryst. Growth* **1974**, *18*, 111.
(5) Hoffman, J. D.; Guttman, C. M.; DiMarzio, E. A. *Discuss. Faraday Chem. Soc.* **1979**, *68*, 177, 378.
(6) Hoffman, J. D. *Polymer* **1982**, *23*, 656.
(7) Hoffman, J. D. *Polymer* **1983**, *24*, 3.
(8) Phillips, P. J. *Polym. Prepr. (Am. Chem. Soc. Div. Polym. Chem.)* **1979**, *20*, 438. 9.
(9) Hoffman, J. D.; Miller, R. L. *Macromolecules* **1988**, *21*, 3038.
(10) Phillips, P. J.; Vatansever, N. *Macromolecules* **1987**, *20*, 2138.

(11) Lovinger, A. J.; Davis, D. D.; Padden, F. J., Jr. *Polymer* **1985**, *26*, 1595.
(12) Cheng, S. Z. D.; Chen, J.; Janimak, J. J. *Polymer*, to be submitted for publication.
(13) Lazcano, S.; Fatou, J. G.; Marco, C.; Bello, A. *Polymer* **1988**, *29*, 2076.
(14) Hoffman, J. D.; Davis, G. T.; Lauritzen, J. I., Jr. In *Treatise on Solid-State Chemistry*; Hannay, N. B., Ed.; Plenum Press: New York, 1976; Vol. 3, Chapter 7.
(15) Vasanthakumari, R.; Pennings, A. J. *Polymer* **1983**, *24*, 175.
(16) Alamo, R.; Fatou, J. G.; Guzman, J. *Polymer* **1982**, *23*, 379.
(17) Organ, S. J.; Keller, A. *J. Polym. Sci., Polym. Phys. Ed.* **1986**, *24*, 2319.
(18) Pelzbauer, Z.; Galeski, A. *J. Polym. Sci., Part C* **1972**, *38*, 23.
(19) Roitman, D. B.; Marand, H. L.; Hoffman, J. D. *Bull. Am. Phys. Soc.* **1988**, *33*, 248.
(20) Barham, P. J.; Keller, A.; Otun, E. L.; Holmes, P. A. *J. Mater. Sci.* **1984**, *19*, 2781.
(21) Clark, E. J.; Hoffman, J. D. *Macromolecules* **1984**, *17*, 878.
(22) Sadler, D. M. *Polymer* **1983**, *24*, 1401.
(23) Sadler, D. M. *Polymer* **1987**, *28*, 1440.
(24) Allen, R. C.; Mandlekern, L. *Polym. Bull.* **1987**, *17*, 473.
(25) Padden, F. J., Jr.; Keith, H. D. *J. Appl. Phys.* **1959**, *30*, 1479.
(26) Norton, D. R.; Keller, A. *Polymer* **1985**, *26*, 704.
(27) Tanabe, Y.; Strobl, G. R.; Fischer, E. W. *Polymer* **1986**, *27*, 1147.
(28) Hoffman, J. D.; Weeks, J. J. *J. Res. Natl. Bur. Std., Sect. A* **1962**, *66A*, 13.
(29) Wunderlich, B. *Macromolecular Physics, Crystal Melting*; Academic: New York, 1980; Vol. 3.
(30) Fatou, J. G. *Eur. Polym. J.* **1971**, *7*, 1057.
(31) Hoffman, J. D.; Miller, R. L. *Macromolecules* **1988**, *21*, 3038.
(32) Bassett, D. C.; Olley, R. H. *Polymer* **1984**, *25*, 935.
(33) Lotz, B.; Wittmann, J. C. *J. Polym. Sci., Polym. Phys. Ed.* **1986**, *24*, 1541.

Flow-Induced Liquid–Liquid Phase Separation and Adsorption Entanglement Layer Formation in High Molecular Weight Polymer Solutions

P. J. Barham* and A. Keller

H. H. Wills Physics Laboratory, University of Bristol, Bristol BS8 1TL, U.K.
Received December 12, 1988; Revised Manuscript Received March 27, 1989

ABSTRACT: Rheological studies of very high molecular weight poly(methyl methacrylate) (PMMA) solutions have revealed three distinct types of anomalous behavior. These are interpreted, at low rates, as being due to the formation of topological adsorption–entanglement layers; at intermediate rates, to the nucleation by adsorption–entanglement layers of a flow-induced liquid–liquid phase separation; and at high rates, to a spontaneous liquid–liquid phase separation. An attempt has been made to construct the phase diagram for the binary system PMMA–dimethyl phthalate by using shear stress, as well as temperature and solution concentration, as thermodynamic variables.

Introduction

There have, over the past 30 or so years, been many reports of anomalous flow behavior in solutions of very high molecular weight polymers (e.g., ref 1–25). In particular in flow systems operating at constant stress (e.g., capillary flows) a decrease in flow rate with increasing flow time has been noted[13–18], and in systems operating at constant flow rate (e.g., Couette flow) the shear stress has been seen to rise during flow[1–10] and in some cases to fluctuate wildly.[10,23,26] It has been shown[18,26–30,32] that such behavior is associated with the formation of layers at surfaces of the viscometers. These layers, which are much thicker than the radius of gyration of polymer molecules, are called "adsorption–entanglement layers" and are believed to be formed by the mutual entanglement of molecules in the flowing solution and those adsorbed along the surfaces.

It has become apparent to us recently that the layers created by flow can be divided into two distinct classes according to their thickness. The first class, type I, as they will be referred to in the following, have a thickness of no more than several micrometers. Such layers are most usually formed in good solvents and at low flow rates. In capillary flow, for example, they cause a decrease in the flow rate, which, after some time, reaches a steady value. These layers can be difficult to detect and, in certain circumstances, can lead to significant error in the actual measurement of viscosity.[31] The second type of behavior (type II) is principally exhibited in poorer solvents at high rates; these layers grow thicker seemingly without limit and can fill the whole flow cell (thicknesses are thus comparable with the dimensions of the equipment and can easily reach several millimeters). Such behavior can result in completely blocked capillaries[27,32] and in Couette and cone and plate geometry leads to dramatic fluctuations in the observed shear and normal stresses.[1–11,26] In such cases some authors also report the observation of "gel-like" particles associated with this behavior (e.g., ref 11).

Recently, Rangel-Nafaile et al.[33] have observed rheological behavior of the same character as type II above, accompanied by the observation of turbidity in the flowing polystyrene solutions. They have consequently attributed their observations, together with many other previous reports on similar rheological observations,[1–23] to a flow induced liquid–liquid phase separation, as opposed to the formation and growth of an adsorption–entanglement layer. Rangel-Nafaile et al. argue that it is the shear stress on the solution that causes a shift in the phase boundaries and leads to liquid–liquid phase separation. The evidence for phase separation comes from observation of turbidity in the solution. Independently, Wolf has come to the same conclusion of liquid–liquid phase

0024-9297/90/2223-0303$02.50/0